ACS OMEGA

http://pubs.acs.org/journal/acsodf

Article

Radiation Synthesis of Carbon/Aluminum/Silica Aerogel Nanoporous Structure Derived from Polyacrylamide Hydrogel for High Temperature and Oil Removal Applications

Mohamed Mohamady Ghobashy,* Ghada Bassioni, Ahmed Zaher, H. Abd El-Wahab, Norhan Nady, Amira El-Sayed, Amr Osman, and Nour El-din Ahmed Abd El-Sattar

Cite This: *ACS Omega* 2023, 8, 20283−20292

Read Online

ACCESS | Metrics & More | Article Recommendations | Supporting Information

ABSTRACT: Aerogel is a high-performance thermal resistance material desired for high-temperature applications like dye-sensitized solar cells, batteries, and fuel cells. To increase the energy efficiency of batteries, an aerogel is required to reduce the energy loss arising from the exothermal reaction. This paper synthesized a different composition of inorganic−organic hybrid material by growing the silica aerogel inside a polyacrylamide (PAAm) hydrogel. The hybrid PaaS/silica aerogel was synthesized using different irradiation doses of gamma rays (10−60 kGy) and different solid contents of PAAm (6.25, 9.37, 12.5, and 30 wt %). Here, PAAm is used as an aerogel formation template and carbon precursor after the carbonization process at a temperature of (150, 350, and 1100 °C). The hybrid PAAm/silica aerogel was converted into aluminum/silicate aerogels after soaking in a solution of $AlCl_3$. Then, the carbonization process takes place at a temperature of (150, 350, and 1100 °C) for 2 h to provide C/Al/Si aerogels with a density of around 0.18−0.040 gm/cm^3 and porosity of 84−95%. The hybrid C/Al/Si aerogels presented interconnected networks of porous structures with different pore sizes depending on the carbon and PAAm contents. The sample with a solid content of 30% PAAm in the C/Al/Si aerogel was composed of interconnected fibrils whose diameter was about 50 μm. The structure after carbonization at 350 and 1100 °C was a condensed opening porous 3D network structure. This sample gives the optimum thermal resistance and a very low thermal conductivity of 0.073 (w/m·k) at low carbon content (2.71% at temperature 1100 °C) and high ν_{pore} (95%) compared with carbon content 42.38% and ν_{pore} (93%) which give 0.102 (w/m·k). This is because at 1100 °C, the carbon atoms evolve to leave an area between Al/Si aerogel particles, increasing the pore size. Furthermore, the Al/Si aerogel had excellent removal ability for various oil samples.

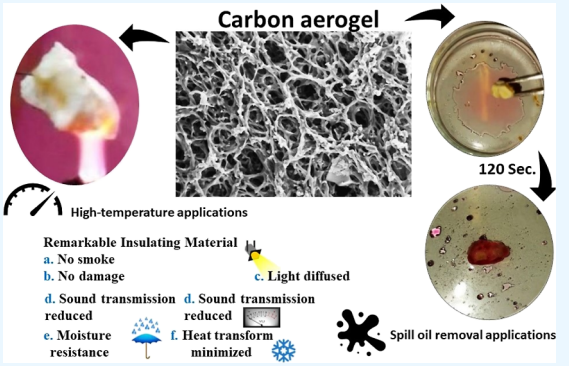

1. INTRODUCTION

Over the last 2 decades, the rapid advancement of sol−gel technologies has resulted in rapid advances in the purposeful production of porous materials.[1] These approaches supplement traditional methods for producing amorphous solids, like impregnation or precipitation processes followed by high-temperature processes.[2] Because of their large surface area, porosity, changeable structure, and surface characteristics, porous materials are critically important in different applications, including adsorption, sensing, and catalysis.[3] Aerogel is defined as a solid porous material due to its porous network structure, high surface area, and high optical transmission.[4] Furthermore, among different kinds of aerogels, silica aerogel has grown in popularity due to a wide range of exceptional physicochemical properties like low thermal conductivity (0.01 W/m·K), high porosity (99%), high optical transmission (99%), high surface area (1000 m^2/g), small dielectric constant (1.0−2.0), low refractive index (1.05), and reduced sound velocity (100 m/s). Silica aerogel is an inorganic amorphous compound with extremely high porosity, high surface area, low density, and low thermal transfer.[5] However, because of their low mechanical strength, silica aerogels possible uses are restricted.[6]

Nevertheless, silica aerogels allow for the simple inclusion of diverse chemicals into their structure, creating materials with distinct physicochemical properties from the original silica aerogels.[7] Several authors have conducted substantial research in the recent decade on the inclusion of particles, polymers, or fibers to improve the mechanical, optical, or thermal properties of silica aerogel.[8] A more modern option is introduced to

Received: November 17, 2022
Accepted: January 26, 2023
Published: May 30, 2023

modify silica aerogel with carbon particles such as carbon nanotubes, carbon nanofiber, graphene, and graphite. The carbon nanostructure has well-established properties like low thermal conductivity and strong mechanical stability. Carbon materials are being actively used in electrode materials due to their excellent electrical conductivity, high specific surface area, and abundant pore structure.[9] Carbon atoms can dope several metals and metal oxides such as charcoal[10] to form hybrid nanocomposites[11,12] for flexible energy storage supercapacitor electrode materials.[13] Mixing the carbon element with silica aerogel can result in novel materials with unique physicochemical properties such as electrochemical, thermal, and adsorption characteristics that can be used in various sectors, including electronics, insulation, and wastewater treatment. Insulation materials typically have a less thermal coefficient of 0.2. The use of insulation materials in manufacturing and construction applications can sometimes have a dramatic effect. Every ton of mineral wool insulating materials used in construction applications over a year may save a ton of petroleum oil.[14] Simultaneously, adopting superior insulating materials in industrial production may significantly cut production consumption of energy and the cost of equipment, resulting in significant economic benefits.[15] Aerogel is regarded as the lightest and the best porous substance as a super insulation material, with unrivaled superiority over other insulation materials.[16] The hybrid carbon−silica aerogel materials are called inverted composites that have a wide variety of uses.[17] For example, adding carbon atoms reduces silica aerogels' thermal conductivity due to infrared radiation absorption caused by carbon broadband absorption for different applications.[18]

Several conventional procedures have been used for oil-water separation, most notably centrifugation, filtration, flotation, gravity separation, biodegradation, and so forth. However, these treatments have intrinsic drawbacks, such as lower efficacy, difficult treatment processes, high costs, or the need to produce additional containments during operation [8]. Sorption, a relatively recent process that has shown to be extremely promising in removing contaminants, was another potent technology [9]. Thus, different absorbers have been investigated, including numerous inorganic sorbents, naturally occurring organic sorbents, and so forth. These absorbers do have certain drawbacks, though. For instance, inorganic sorbents displayed some intrinsic limits due to their high density and low oil sorption capabilities.[19,20] The bulk of naturally occurring organic sorbents had a low hydrophobicity, or capacity to repel water, which led to high water uptake. Development of novel sorbents with advantages in sorption capacity, selectivity, density, recyclability, hydrophobicity, lipophilia, and environmental friendliness was therefore necessary. This article synthesizes composites of ammonium/silica aerogel-based carbon atoms. It is made up of three major sections: first, it provides a summary of the key phases of polyacrylamide (PAAm) hydrogel synthesis by gamma irradiation techniques. The usual technique and eco-friendly methods of gamma irradiation are used to prepare a cross-linked hydrogel.[21−26] Second, the essential features of aluminum silica aerogels have been described and how they may be produced. Finally, the incorporation of carbon elements into aluminum silica aerogels and the uses of the resultant composites have been discussed. Aerogel samples are tested and compared to remove six common kinds of oils. Thus, this work aims to demonstrate current developments in adding carbon into aluminum silica aerogels and their impact on high-temperature and oil removal applications.

2. EXPERIMENTAL AND MATERIAL

Sigma-Aldrich Co. provided acrylamide monomer (AAm) with a purity of 99%. The silica precursor is liquid sodium silicate (Na_2SiO_3) acquired from Egypt Global Silicates Co., Ltd. (Egypt) with a SiO_2/NaO ratio of 3.1−3.4 in the water glass. Bi-distilled water and all reagents were utilized in this study with no additional purification.

2.1. Methods of Preparation of Carbon/Aluminum/Silica Aerogel. The carbon/aluminum/silica aerogel investigated in this paper was derived by carbonization of the PAAm precursor at three different temperatures (150, 350, and 1100 °C). The synthesis of hybrid hydrogel/aerogel is described in detail in our previous paper.[27] Due to acrylamide being a neutral compound, sodium salt is not formed when it reacts with Na_2SiO_3.[28,29] Briefly, irradiation methods were used to create the carbon precursor (PAAm) by dissolving (Am) monomers in an aqueous solution of sodium silicate (Na_2SiO_3) as a silicate precursor. The PAAm hydrogel templates were created by dissolving 10 g of AAm (CH_2═$CHC(O)NH_2$) in 160 mL of distilled water, yielding a solution (A) with a 6.25 percent dissolved solid content. Sodium silicate (100 mL) labeled as a solution (B) is a silicon precursor. Then, a dropwise addition of precursor solutions (B) and (A) was performed with continuous stirring. After around 60 min, the combined (A + B) solutions were filtered to guarantee that a perfectly homogeneous solution was achieved. The polymerization process was then carried out utilizing the gamma irradiation approach. The mixed solution was placed into a polyethylene bag and treated with six gamma radiation dosages: (10, 20, 30, 40, 50, and 60 kGy). These processes resulted in developing a cross-linked PAAm hydrogel with sodium silicate inside the hydrogel matrix to give (PAAm-Si). The disk-shaped (PAAm-Si) was then submerged in a saturated solution of $AlCl_3$ with vigorous stirring to initiate sodium silicate hydrolysis (silicon precursor). After around 90 min, the PAAm disc was transferred to a fresh $AlCl_3$ solution to speed up hydrolysis. This procedure was performed three times, and the PAAm disc was immersed in $AlCl_3$ solution for 24 h. The color of the PAAm hydrogel then changes to white, indicating the production of Al-silicate inside the (PAAm) hydrogel to give (PAAm/Al-silicate). The PAAm/Al-silicate was removed from the hydrolyzed solutions and put in an oven at three different temperatures (150, 350, and 1100 °C) for 2 h to carbonize. The carbonization technique avoids Al-silicate shrinkage while providing a porous structure for (C/Al/Si) aerogel with excellent mechanical strength. Finally, the produced (C/Al/Si) aerogel was stored dry for future research. The above processes were performed with AAm monomer at different weights of 9.37, 12.5, and 30%. The Al-silicate aerogel was synthesized with varied PAAm solid concentrations (6.25−30 wt %). Before the carbonization process, the washing step effectively removes Na and Cl contaminant elements.

2.2. Kinetic Swelling Studies. The swelling kinetics were investigated to understand the diffusion process of water molecules into the PAAm hydrogel samples. Equation 1 was utilized to process the kinetic data of the swelling process to get information on the mechanism of water transport through the hydrogels based on the good adaptation of swelling data of PAAm hydrogel samples with Fick's laws.

https://doi.org/10.1021/acsomega.2c07335
ACS Omega 2023, 8, 20283−20292

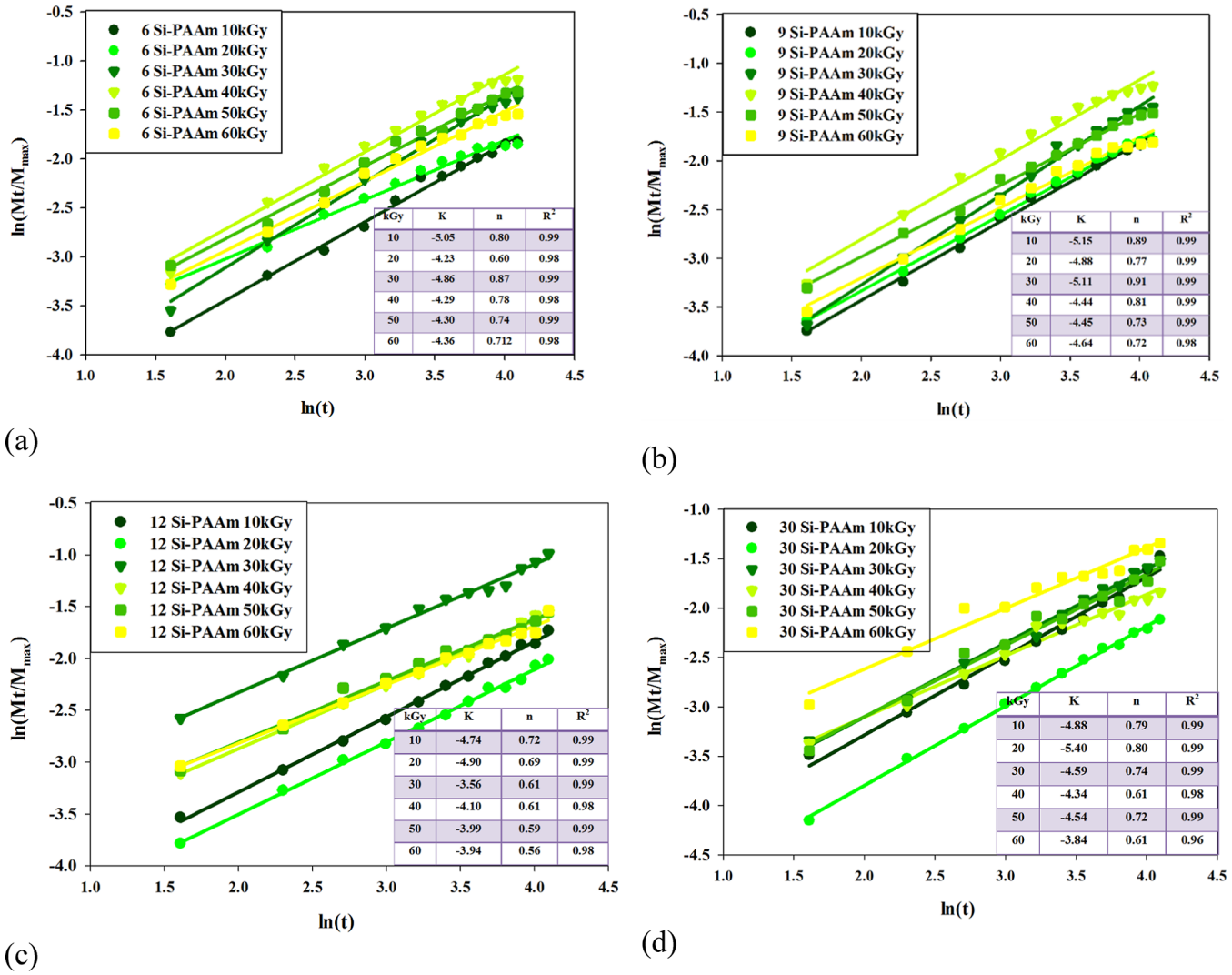

Figure 1. PAAm hydrogels samples (a) 6.25, (b) 9.37, (c) 12.5, and (d) 30 wt % at different irradiation doses (10 up to 60 kGy).

$$\frac{M_t}{M_\infty} = Kt^n \tag{1}$$

where M_t and M_∞ are the water mass absorbed at the time (t) and the water mass absorbed at equilibrium, respectively, and k (min) and "n" are the kinetic constant of the hydrogel swelling and the mechanism of water transport. Fickian diffusion and Case II (relaxation-controlled) transport are defined by n values of 0.5 and 1, respectively. Non-Fickian or anomalous transport is between Fickian and Case II ($0.5 < n < 1$).

2.3. Measurements of Swelling Properties. The swelling degree (g/g) of silica PAAm (PAAm/Si) was calculated by the following equation

$$\text{swelling degree(g/g)} = (W_t - W_o)/W_o \tag{2}$$

W_t is a given swelling weight of the Si-PAAm hydrogel sample at every 5 min and W_o is the initial dry weight of the (PAAm/Si) hydrogel sample.

2.4. Density and Pore Volume (%) of (C/Al/Si)-Aerogel at Different Carbon Contents. The Archimedes method was used to calculate the density (d) of (C/Al/Si)-aerogel samples made by adding $AlCl_3$ to Si-PAAm hydrogel before carbonization. The test settings for all samples were kept similar during the density test. The experiment was performed three times before taking the mean result to calculate the final density (d). The dry (C/Al/Si)-aerogel samples weights (w_1) and submerged the (C/Al/Si)-aerogel samples in water and the weights (w_2) were recorded.

The density (d) (g/cm^3) of the C/Al/Si aerogel sample was calculated using eq 3

$$D = (w_1/w_1 - w_2)\cdot d_w \tag{3}$$

The density of water (1.003 g/cm^3, 25 °C, 1 atm) is written as d_w.

The air percentage (V_{pore} %) of a (C/Al/Si)-aerogel sample was measured by subtracting the volume (V_1) of a rectangular sample (C/Al/Si)-aerogel from its (m_1) weight for each (C/Al/Si)-aerogel sample using eq 4 below

$$V_1 = L \times H \times W(\text{cm}^3) \tag{4}$$

L, H, and W are the length, height, and width of the rectangular shape of the (C/Al/Si)-aerogel sample, respectively. The volume of air is V_{pore}, the volume of the whole sample is V_1, and m_1 is the weight of the (C/Al/Si)-aerogel sample as shown in eq 5.

$$\%V_{pore} = V_1 - m_1 = V_{pore}\cdot 100 \tag{5}$$

https://doi.org/10.1021/acsomega.2c07335
ACS Omega 2023, 8, 20283−20292

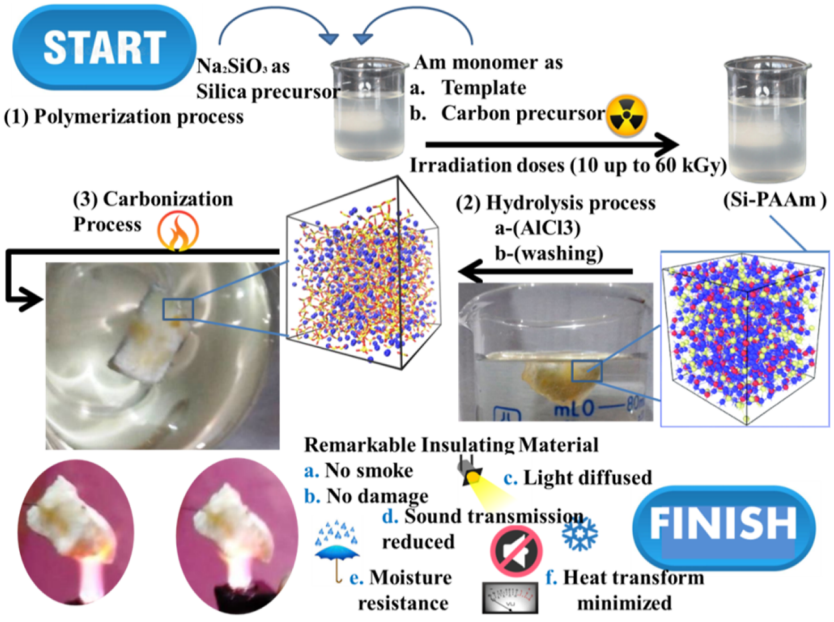

Figure 2. Process of carbon/aerogel preparation.

Then, the volume (V %) of the (C/Al/Si)-aerogel is calculated by eq 6

$$V\ \% = 100 - \%\ V_{\text{of air}} \tag{6}$$

The weight loss W_l (%) was calculated after the removal of the organic components as shown in eq 7

$$W_l = 100 - ((W_i/W_o)\cdot 100) \tag{7}$$

The W_i and W_o are the weights of (C/Al/Si) aerogel and (PAAm/Si) hydrogel after and before the carbonization at the temperature of 1100 °C for 2 h, respectively.

2.5. Scanning Electron Microscopy. A field emission scanning electron microscope (Nova Nano scanning electron microscope) 430 m, FEI, Czech Republic, The Netherlands) was used to investigate the network architecture, the pore size, and the microstructure of (C/Al/Si)-aerogel samples and their symmetry for varied PAAm solid contents followed the carbonization process of the (C/Al/Si)-aerogel samples at temperatures of 150, 350, and 1100 °C. The energy-dispersive X-ray (EDX) analysis and mapping mode was used for element detections for the (C/Al/Si)-aerogel samples carbonized at a temperature of 1100 °C.

2.6. Fourier-Transform Infrared Spectroscopy. The chemical structure of (C/Al/Si)-aerogel samples was determined using an attenuated total reflectance−Fourier transform infrared (ATR−FTIR) Vertex 70 FTIR spectrometer coupled with a HYPERIONTM series microscope (Bruker Optik GmbH, Ettlingen, Germany). The FTIR scan runs from 4000 to 400 cm^{-1} with a resolution of 4 cm^{-1}. The FTIR data are processed using the program OPUS 6.0. (Bruker).

2.7. Thermal Conductivity Measurement. A (C/Al/Si)-aerogel samples were measured using a KD2 Pro thermal conductivity instrument with a transient line heat source. The KD2 Pro is a field and lab thermal properties analyzer tool that measures the thermal conductivity of porous materials. The accuracy of the data gathered for thermal conductivity, diffusivity, and resistivity varied from 5 to 10%. Thermal conductivity tests were traditionally performed using a probe consisting of a needle with a heater and temperature sensor inside. The needle is submerged in (C/Al/Si)-aerogel sample for around 6 mm dipping. The submerged needle is heated for a predetermined amount of a certain record time.

3. RESULTS AND DISCUSSION

3.1. Swelling Kinetics of PAAm Hydrogels. When the solid content of the PAAm hydrogels increases, the intermolecular interactions and the porosity structure of PAAm hydrogels reach their maximum.[27] The swellability of the PAAm hydrogels becomes dependent on the solid content. Figure 1a−d shows the plot $\ln(M_t/M_\infty)$ versus $\ln(t)$ for the swelling behavior of all PAAm hydrogels samples (6.25, 9.37, 12.5, and 30 wt %) at different irradiation doses (10−60 kGy) and ambient temperature. For all hydrogel samples, the linear curve (R^2 = 0.99) of swelling kinetics indicates that a Fickian mechanism controls the swelling behavior of PAAm hydrogels. According to Figure 1a−d and swelling exponent "n" values, the swelling behavior of all (PAAm) hydrogel samples is typically fitted to the non-Fickian behavior. Because 30% PAAm hydrogel possesses more solid content in its network structure than other PAAm samples, the swelling behavior may be the lowest than the other PAAm hydrogel samples and slow down the relaxation of macromolecular chains, resulting in the lowest water content and lowered swelling exponent "n" values than all other PAAm samples. Moreover, the irradiation dose applied to the swelling behavior of PAAm samples results in a non-Fickian process.

At a low irradiation dose 10 kGy, the PAAm hydrogel sample shows the highest swelling behavior due to the largest porous size. Moreover, high irradiation doses (60 kGy) showed the lowest swelling behavior among the other irradiation doses due to the high density of crosslinked network that slowed down the relaxation of macromolecular chains. These results of swelling kinetics confirm that PAAm hydrogels at high solid content and high irradiation doses have a more compact and condensed network structure than other samples.

3.2. Carbonization Process of (PAAm/Si) Aerogel to form Carbon Aerogel. The percent work novelty lies in preparing carbon/aluminum aerogels by polymerizing acryl-

https://doi.org/10.1021/acsomega.2c07335
ACS Omega 2023, 8, 20283−20292

amide dissolved in sodium silicate solution as carbon precursors and silica precursors, respectively, followed by a carbonization process. Figure 2 outlines the procedures for forming carbon/aluminum aerogels.

At the polymerization process, the PAAm hydrogel is formed by crosslinking (Am) monomers dissolved in sodium silicate using different gamma irradiation doses of (10−60 kGy). This gives the hydrogel/aerogel (Si/PAAm) a three-dimensional (3D) porous network structure, where the hydrogel here is used as the template. Thus, the resulting (PAAm/Si) is structurally controllable by the content of Am monomers.

During hydrolysis, the obtained (Si/PAAm) hydrogel is kept in a solution of $AlCl_3$. The hydrolysis step is a critical step for aerogel preparation. In this step, the sodium silicate consisting of the PAAm hydrogel network is changed, leaving only the solid network of Al/Silicate/PAAm, that is, hydrogel/Al-aerogel is formed. This process is important to find the final structure and study aerogel properties. Three cycles of hydrolysis by $AlCl_3$ and washing to remove Na ions, as shown in Figure 2.

During the carbonization process, the obtained Al/Silicate/PAAm aerogel is heated to 1100 °C under ambient conditions. PAAm moieties are decomposed into carbon and trapped inside the Al/Si/aerogel to form the C/Al/Si/aerogel. Notably, the carbonization temperature at temperatures 150, 350, and 1100 °C significantly forms carbon/aerogels at different carbon contents. In addition. The physical properties of aerogels are significantly changed in this stage. For example, aerogels become moisture resistant, reduce sound transmissions, have light diffusivity, have no smoke production, and have low heat transfer. Generally, the preparation process for most carbon aerogels includes three stages: gelation, hydrolysis, and carbonization (Figure 2) because each step impacts the final results.[30]

3.3. Study the Pore Size Structure of Carbon/Aluminum/Silica (C/Al/Si)-Aerogel. Scanning electron microscopy (SEM) pictures of PAAm/aerogel samples prepared at irradiation doses of 30 kGy and their carbonization at different temperatures (150, 350, and 1110 °C) to give carbon/aluminum-silica/aerogel (C/Al/Si)-aerogel is shown in Figure 3. The 3D network of all (C/Al/Si)-an aerogel with a pore diameter in the range of 2−40 μm can be observed in Figure 3.

In general, the pore diameter is decreased with a wide-ranging distribution for all (C/Al/Si)-aerogel samples carbonization at the temperature of 150, 350 °C in which the pore diameter is comparatively small with a narrower size distribution compared to (Al/Si)-aerogel (samples carbonization at the temperature of 1100 °C). At the high level of carbon, the network of (C/Al/Si)-aerogel samples is more compact and thus more interconnected, while the porosity remains small.

SEM micrographs of the (Al/Si)-aerogel at different solid contents (6.25, 9.37, 12.5, and 30%) showed a homogeneous and largest porous and interconnected 3D network structure, which was formed during the carbonization at a temperature of 1100 °C. Figure 3d1 shows the (C/Al/Si)-aerogel of 30% PAAm that consisted of interconnected fibrils whose diameter was about 50 μm. After carbonization at 350 and 1100 °C, it was obvious that the porous 3D network was condensed (Figure 3d2,d3). However, compared with the (C/Al/Si)-aerogel of 6.25, 9.37, and 12.5% PAAm, the structure of the carbon aerogel expanded and the pore size increased, giving

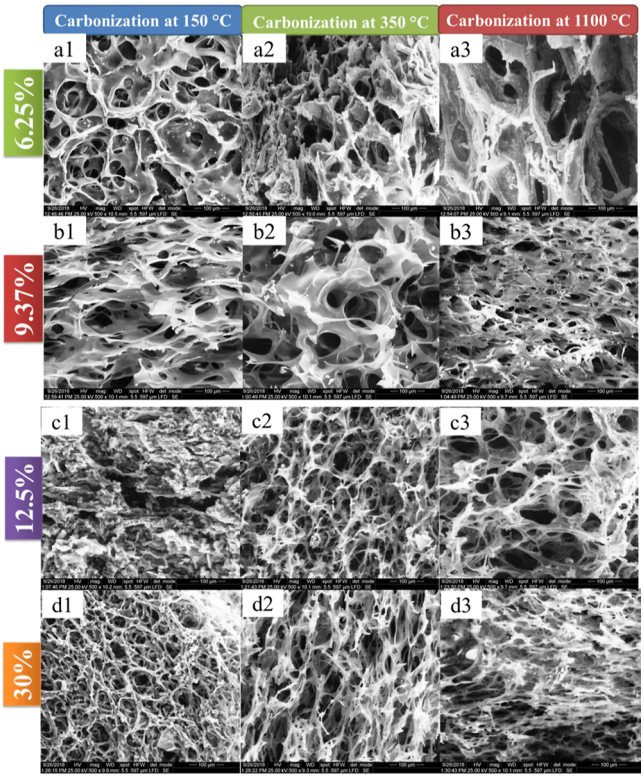

Figure 3. SEM images of (C/Al/Si)-aerogel samples prepared at different contents of PAAm, (a) 6.25, (b) 9.37, (c) 12.5, and (d) 30 wt %, and carbonization temperatures.

rise to bigger pore diameter after carbonization at 350 and 1100 °C. As shown in Figure 3d3, the SEM image of (Al/Si)-aerogel of 30% PAAm sample has sheets stacked densely to build a wrinkled shell surface and link to make a porous portion surrounded by the thick shell.

According to the picture on the left, Figure 3 demonstrates the SEM image of a cross-linked (C/Al/Si)-aerogel. The (Al/Si)-aerogel represents the less cross-linked silica aerogel due to the carbonization process temperature of 1100 °C that leads to the evolution of carbon atoms that can destroy the primary cross-linked silica aerogel network and form cluster particles of (Al/Si) that arrange themselves in a shelves-like structure with big size of pores formed. This means that the PAAm polymer successfully forms a network pore structure in the prepared (C/Al/Si)-aerogel and (Al/Si)-aerogel. Moreover, the porous network shaped in (C/Al/Si)-aerogel cannot remain as an aerogel after carbonization but is changed. It can be seen from Figure 3, the porous structure is still present in the (Al/Si) aerogel after carbonization at a temperature of 1100 °C but the inner skeleton of the aerogel and the framework becomes thicker and sharper. Moreover, the pore volume becomes larger than (C/Al/Si) aerogel samples.

It can be seen in Table 1 that the porous structure of the prepared (C/Al/Si)-aerogel is strongly dependent on the content of carbon. (C/Al/Si)-aerogel of 30% PAAm sample has an optimal porous structure that gives the lowest density of 0.04 gm/cm^3 after the carbonization process at 1100 °C. It can be concluded that the (C/Al/Si)-aerogel of the 30% PAAm sample has the largest V_{pore} and the lowest density.

One of the most significant key factors in determining the physical characteristics of carbon aerogels is the carbonization temperature. Lin and Ritter[30] noted that when the temperature

https://doi.org/10.1021/acsomega.2c07335
ACS Omega 2023, 8, 20283−20292

Table 1. Values of Density and Pore Volume of Aerogel Samples at Different PAAm Contents and Carbonization Temperatures

	(6.25%)		(9.37%)		(12.5%)		(30%)	
carbonization temperature (°C)	d (gm/cm^3)	V_{pore} (%)	d (gm/cm^3)	V_{pore} (%)	d (gm/cm^3)	V_{pore} (%)	d (gm/cm^3)	V_{pore} (%)
150	0.18	84.50	0.16	86	0.10	81	0.081	92
350	0.14	87	0.13	87.5	0.12	88	0.084	93
1100	0.12	88	0.25	89	0.09	90	0.04	95

is below 600 °C, temperature fluctuations have no substantial effect on the specific surface area of the aerogel. When the temperature is between 700 and 900 °C, the pore volume decreases with the increase in temperature. However, the pore volume is not changing clearly with the temperature increase beyond 900 °C.

As mentioned above, the structure of the carbon aerogel expanded and the pore size increased due to the possibility of escaping the oxygen and hydrogen elements from the aerogel framework.

Yamamoto et al.[31] used the sol−gel polycondensation of formaldehyde and resorcinol in an alkaline aqueous solution, followed by freeze-drying to create a composite of carbon aerogel. He and his co-workers discovered that the mesopore and micropore in aerogel grow as the macropore decreases. Furthermore, the carbonization procedure greatly increases the specific surface area. The oxygen and hydrogen groups may escape from the framework, creating a new small hole. Figure 4

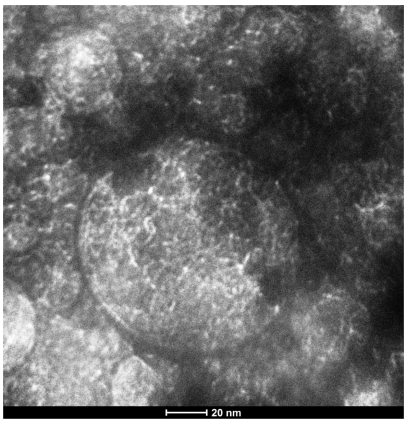

Figure 4. TEM image of 30 (Al/Si/PAAm)-30 kGy sample after carbonization at 1100 °C.

shows the nanoporous structure of the obtained (C/Al/Si) aerogel after carbonization of 30(Al/Si/PAAm)-30 kGy samples at a temperature of 1100 °C. Figure 4 show the pore size is 2 nm due to the carbonization process.

3.4. Effect of Carbonization Temperature on the Chemical Structure of PAAm/Aerogel Samples. The chemical structure of PAAm/aerogel samples and corresponding carbon/aerogel after the carbonization process were studied using FTIR/ATR, as shown in Figure 5. As represented in Figure 5a, the FTIR spectrum of the PAAm/aerogel at 150 °C shows a peak at 3300 cm^{-1} attributed to O−H groups in PAAm molecules. The observed peaks at 1654 and 1561 cm^{-1} are attributed to stretching vibration C═O and deformation vibrations of N−H of amide groups.[32] The peak located at 1030 cm^{-1} is assigned to the C−O bond. The FTIR peak at 1425 cm^{-1} is attributed to the amide group's C−N stretching vibration. After the carbonization at a temperature

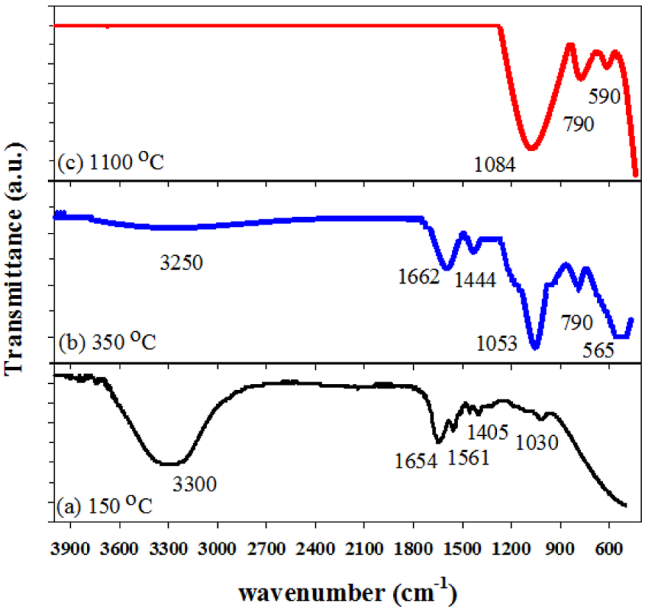

Figure 5. FTIR/ATR of PAAm/aerogel samples and corresponding carbon/aerogel after the carbonization process at temperatures of (a) 150, (b) 350, and (c) 1100 °C.

of 350 °C, the peaks of PAAm molecules such as O−H, C═O, C−N, and N−H become significantly weaker and some peaks disappear, as displayed in Figure 5b. This is due to the decomposition process of groups in the carbonization process at 350 °C. The FTIR peak located at 790 cm^{-1} is attributed to Si−CH$_3$ and the broadband around 1053 cm^{-1} shows typical Si−O contributions in silica aerogels[33] and FTIR located at 565 cm^{-1} attributed to the bending vibration of Si−O−Al. After the carbonization at the temperature of 1100 °C, the peaks of PAAm molecules such as O−H, C═O, C−N, and N−H completely disappear, as shown in Figure 5c. The FTIR peak located at 790 cm^{-1} is attributed to Si−CH$_3$ and the peak located at 1084 cm^{-1} and 590 are typical to Si−O and Si−O−Al bending vibration contributions in aluminum silica aerogels.[34]

For further investigation, EDX elemental analysis of the 30% PAAm/aerogel was performed at different temperatures of carbonization (Figure 6). Figure 6a shows that the principal four elements are C, Si, O, and Al, with minor levels of Na (1.68 At %) and Cl (2.21 At %), showing that the Na and Cl ions have been successfully removed by solvent exchange. The Na and Cl do not appear in the EDX chart in Figure 6b,c, suggesting that the Na and Cl inside the aerogel matrix from the PAAm matrix have been fully eliminated due to the calcination process (350 °C). This demonstrates that pure C/Al/Si aerogels can be made and that contaminants are eliminated throughout the carbonization procedures. The results indicate that at carbonization temperatures of 150, 350, and 1100 °C, the carbon contents are 39.54, 42.38, and

https://doi.org/10.1021/acsomega.2c07335
ACS Omega 2023, 8, 20283−20292

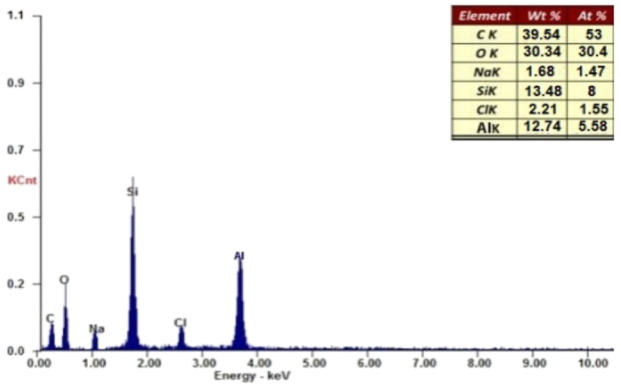

(a) 150°C

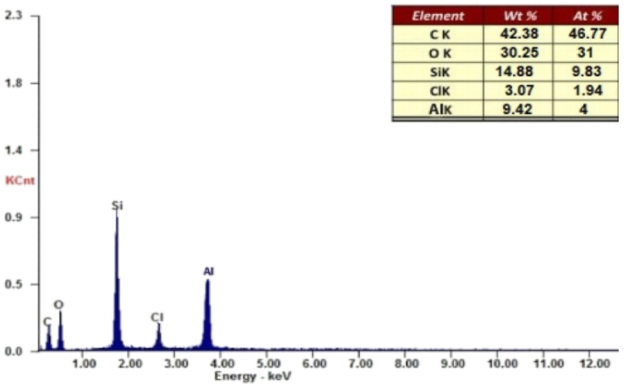

(b) 350 °C

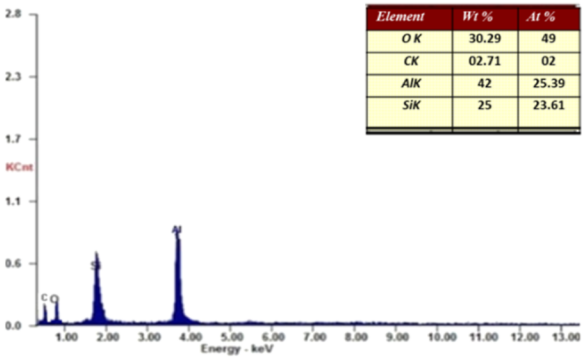

(c) 1100 °C

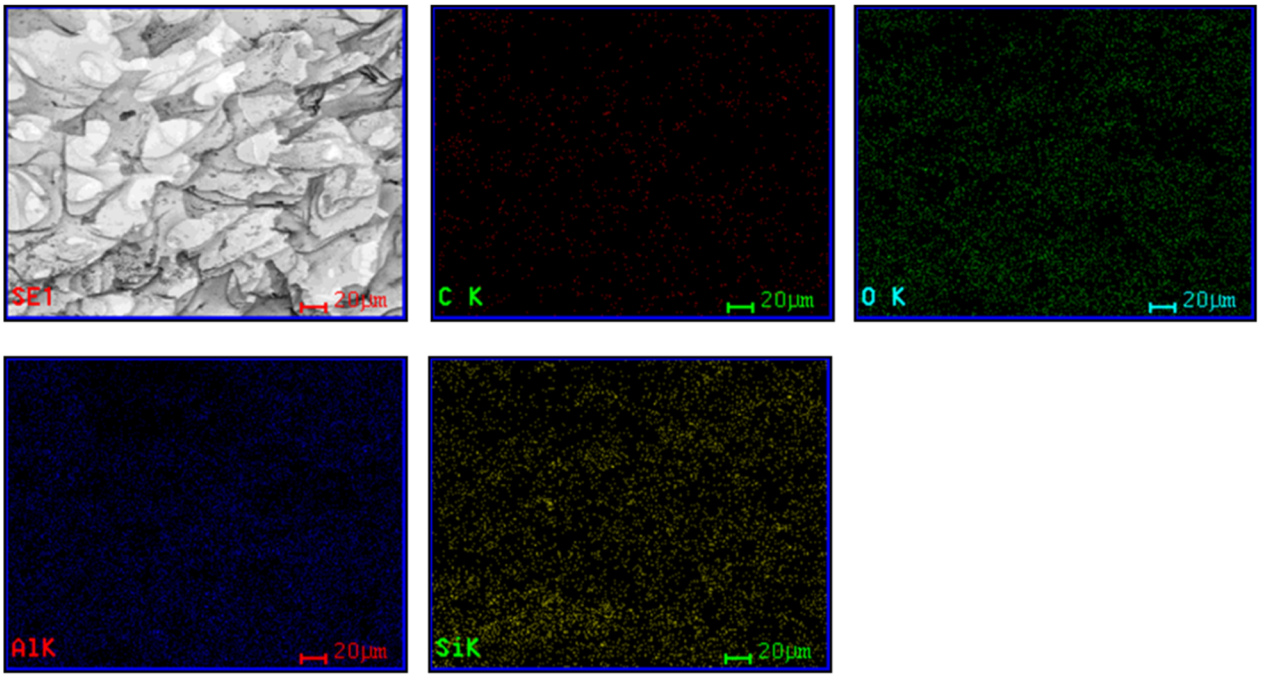

(d)

Figure 6. EDX charts of Al-(Si-PAAm) ignited at different temperatures of (a) 25, (b) 250, and (c) 1100 °C and (d) the mapping of the (C/Al/Si)-aerogel.

https://doi.org/10.1021/acsomega.2c07335
ACS Omega 2023, 8, 20283−20292

2.71 At %, respectively. As expected, the content of C is temperature-dependent. Figure 6d shows the mapping of all the necessary components belonging to both phases are homogeneously distributed in the examined locations, demonstrating a homogeneous combination of silica, aluminum, and carbon elements.

3.5. Effect of Carbon Content on the Thermal Conductivity for the (Al−Si) Aerogel. The current work primarily concerns the thermal insulation performance of various Al−Si aerogel composites. The impact of carbon filler on the thermal characteristics of silica aerogels is seen in Figure 7. The obtained (Al−Si) aerogel materials with porous

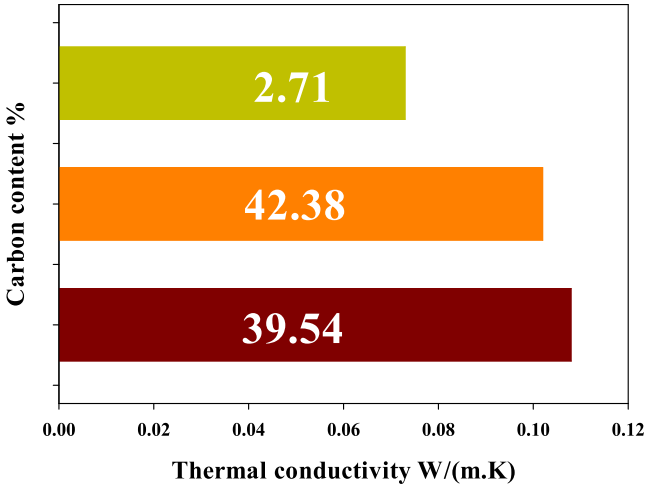

Figure 7. Thermal insulating performance of (Al/Si)-aerogel in correlation with the carbon content.

structures consist of distributed two-phase materials (carbon and air). The carbon content correlates with the thermal connectivity of the aerogel, where the increase of carbon content leads to an increase in the thermal conductivity of the aerogel. Several studies confirmed that the thermal conductivity of aerogels rises after doping with other elements.[34,35] In addition, Guo, Donghui, et al.[36] and Shan, Hui, et al.[37] reported that C doping could induce and prompt the porous structure formation during the doping process of aerogel materials, besides the effects of chemical composition. The density and volume percentage of the pore on the thermal conductivity are investigated in Table 2. The thermal conductivity value *K* depended on the volume pore %. With the increase in porosity, the thermal conductivity of aerogel samples decreases.[38]

3.6. Absorption Capacity of Different Oils by (C/Al/Si)-Aerogel. The obtained (C/Al/Si)-aerogel sample calcined at 1100 °C were further tested by examining their adsorption for different oils. Figure 8 showed that the (Al/Si)-aerogel had various oil adsorption capacity (crude oil, engine oil, hydraulic

Table 2. Results of Thermal Conductivity of the Al-Silica Aerogel

studied samples	V_{pore} (%)	*d* (gm/cm^3)	C content %	thermal conductivity *K*-value W/(m·K)
150	92	0.081	39.54	0.108
350	93	0.084	42.38	0.102
1100	95	0.040	2.71	0.073

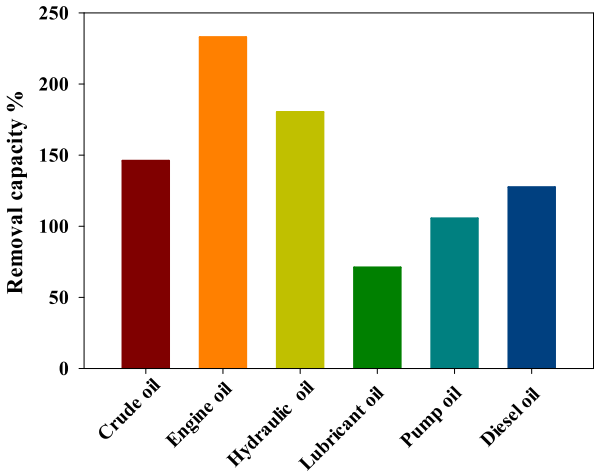

Figure 8. Adsorption capacity of six oil samples by the (C/Al/Si)-aerogel.

oil, lubricant oil, pump oil, and diesel oil) under ambient conditions. It can be seen that the adsorption capacity of the (C/Al/Si)-aerogel is in the range of 70−232 times higher than its weight for various oils (Figure 8). The absorption ratios of crude oil, engine oil, hydraulic oil, lubricant pump oil, and diesel oil were different. The oil absorption capacity of crude oil was higher 145 times, engine oil's absorption capacity was 232 times, while hydraulic oil had an absorption capacity 180 times. The oil absorption capacity of lubricating oil was the smallest with 70 times, pump oil's absorption capacity was 105 times, while diesel oil had an absorption capacity 172 times. The oil was mainly stored in the macropores of the aerogel, so the difference in the absorption capacity between the various oils depended on the surface tension and density of the solvent tested and the different porous structures and porosities inside the aerogel samples. Capillary forces were responsible for the adsorption capacity of aerogels. Due to the capillary interaction between the mobile oil and the aerogel surface, the oil could flow spontaneously into the narrow network channel inside the aerogel. Engine oil's absorption capacity was higher than most existing oil absorption materials.

Engine oil removal tests were also performed to investigate the ability of the (C/Al/Si)-aerogel to separate and adsorb engine oils (Figure 9). Almost all of the engine oil was successfully separated rapidly within 2 min of exposure. It can be seen that water is not adsorbed by the (C/Al/Si)-aerogel sample in Figure 9 and aerogel floating on the water due to the low mean density, the aerogel floated on the upper part of water and oil mixtures after the engine oil was extracted completely, indicating that the system designed in this study is feasible for use in chemical spillages and elimination of oil leaks. Thus, these aerogels show great promise in separating dirt and oils from water due to their hydrophobicity, mechanical consistency, and high porosity.

4. CONCLUSIONS

The irradiation technique is good for preparing hydrogel/aerogel based on PAAm. The PAAm hydrogel is formed by crosslinking (Am) monomers dissolved in sodium silicate. A non-Fickian process controls the swelling behavior of the PAAm sample. The current work primarily concerns the thermal insulation performance of various Al−Si aerogel composites according to the C element content. The obtained

https://doi.org/10.1021/acsomega.2c07335
ACS Omega 2023, 8, 20283−20292

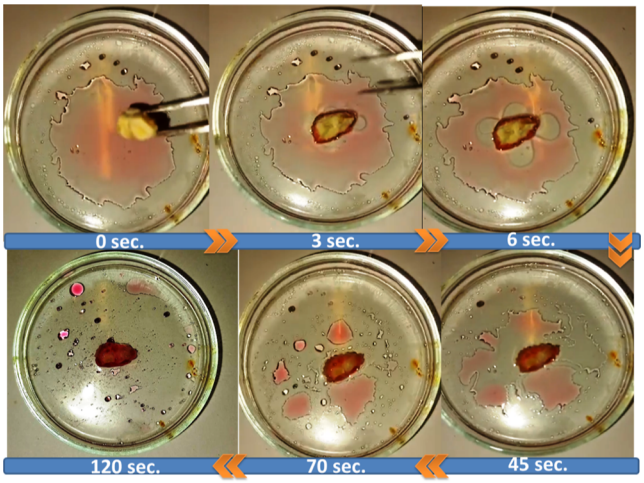

Figure 9. Removal of engine oil (dyed with Sudan red) in 120 s from the water surface using the (C/Al/Si)-aerogel sample.

results confirm that the obtained carbon/aerogel at high solid content and high irradiation doses have a more compact network structure than other samples. Hydrolysis and carbonization steps are critical steps for carbon/aerogel preparation. PAAm moieties are decomposed at 1100 °C into carbon and trapped inside the Al/Si/aerogel. Peaks of PAAm molecules such as O−H, C═O, C−N, and N−H disappear after carbonization at 1100 °C. Carbon content affects the thermal connectivity of aerogels: the higher the carbon content, the better the thermal conductivity. The best effect of carbon doping of (2.71) on the thermal properties of silica aerogel gives thermal insulation of (0.04 w/m·k). SEM micrographs of the (C/Al/Si)-aerogel at different solid contents (6.25, 9.37, 12.5, and 30%) showed a homogeneous, porous, interconnected 3D network structure. (C/Al/Si)-aerogel of 30% PAAm sample has an optimal porous structure with the lowest density of 0.04 gm/cm^3 after the carbonization process at 1100 °C. The structure of the carbon aerogel expanded and the pore size increased due to the possibility of escaping oxygen and hydrogen groups upon heating. The results of SEM, transmission electron microscopy (TEM), and mapping confirmed that the porous structure of the obtained (C/Al/Si)-aerogel is a nanoporous structure (2 nm).The largest pore size and lowest density were achieved for the (C/Al/Si)-aerogel is prepared from 30 (Si/PAAm)-30 kGy. This means that the carbon contents are effective on the porosity % of the aerogel samples. The oil adsorption experiments revealed that the (C/Al/Si)-aerogel had excellent adsorption ability of oils in order (engine oil, hydraulic oil, crude oil, diesel oil, pump oil, and lubricating oil).

■ ASSOCIATED CONTENT

Supporting Information

The Supporting Information is available free of charge at https://pubs.acs.org/doi/10.1021/acsomega.2c07335.

Removal of oil from the water surface using the (C/Al/Si)-aerogel sample (MP4)

■ AUTHOR INFORMATION

Corresponding Author

Mohamed Mohamady Ghobashy − *Radiation Research of Polymer Chemistry Department, National Center for Radiation Research and Technology (NCRRT), Egyptian Atomic Energy Authority (EAEA), Cairo 4441501, Egypt;* orcid.org/0000-0003-0968-1423; Phone: +20222727413; Email: Mohamed.ghobashy@eaea.org.eg, Mohamed_ghobashy@yahoo.com; Fax: +20222749298

Authors

Ghada Bassioni − *Faculty of Engineering, Ain Shams University, Cairo 11517, Egypt;* orcid.org/0000-0001-8928-6428

Ahmed Zaher − *Chemistry Department, Faculty of Science, El-Mansoura University, El-Mansoura 35516, Egypt*

H. Abd El-Wahab − *Department of Chemistry Faculty of Science, Al-Azher University, Cairo 387130, Egypt*

Norhan Nady − *Polymeric Materials Research Department, City of Scientific Research and Technological Applications (SRTA-City), Alexandria 21934, Egypt*

Amira El-Sayed − *Department of Chemistry, Faculty of Science, Ain Shams University, Cairo 11517, Egypt*

Amr Osman − *Department of Chemistry, Faculty of Science, Ain Shams University, Cairo 11517, Egypt*

Nour El-din Ahmed Abd El-Sattar − *Department of Chemistry, Faculty of Science, Ain Shams University, Cairo 11517, Egypt;* orcid.org/0000-0001-6680-4448

Complete contact information is available at: https://pubs.acs.org/10.1021/acsomega.2c07335

Notes

The authors declare no competing financial interest.

■ ACKNOWLEDGMENTS

This paper is based on work supported by Science, Technology & Innovation Funding Authority (STDF) under grant number (46339)

■ REFERENCES

(1) Ciriminna, R.; Fidalgo, A.; Pandarus, V.; Béland, F.; Ilharco, L. M.; Pagliaro, M. The sol−gel route to advanced silica-based materials and recent applications. *Chem. Rev.* **2013**, *113*, 6592−6620.

(2) Frenzer, G.; Maier, W. F. Amorphous porous mixed oxides: Sol-gel ways to a highly versatile class of materials and catalysts. *Annu. Rev. Mater. Res.* **2006**, *36*, 281−331.

(3) Chuhadiya, S.; Himanshu, D.; Suthar, S. L.; Patel, M. S.; Dhaka, M. S. Metal organic frameworks as hybrid porous materials for energy storage and conversion devices: A review. *Coord. Chem. Rev.* **2021**, *446*, 214115.

(4) Gao, Y.; Dong, C.; Zhang, F.; Ma, H.; Li, Y. Constructing Polyimide Aerogels with Carboxyl for CO2 Adsorption. *Polymers* **2022**, *14*, 359.

(5) Cheng, H.; Fan, Z.; Hong, C.; Zhang, X. Lightweight multiscale hybrid carbon-quartz fiber fabric reinforced phenolic-silica aerogel nanocomposite for high temperature thermal protection. *Compos. Appl. Sci. Manuf.* **2021**, *143*, 106313.

(6) Iswar, S.; Galmarini, S.; Bonanomi, L.; Wernery, J.; Roumeli, E.; Nimalshantha, S.; Ishai, A. M. B.; Lattuada, M.; Koebel, M. M.; Malfait, W. J. Dense and strong, but superinsulating silica aerogel. *Acta Mater.* **2021**, *213*, 116959.

(7) Lamy-Mendes, A.; Pontinha, A. D. R.; Alves, P.; Santos, P.; Durães, L. Progress in silica aerogel-containing materials for buildings' thermal insulation. *Construct. Build. Mater.* **2021**, *286*, 122815.

(8) Adhikary, S. K.; Ashish, D. K.; Rudžionis, Ž. Aerogel based thermal insulating cementitious composites: A review. *Energy Build.* **2021**, *245*, 111058.

(9) Zhang, Y.; Chang, C.-r.; Jia, X.-d.; Huo, Q.-y.; Gao, H.-l.; Yan, J.; Zhang, A.-q.; Ru, Y.; Mei, H.-x.; Gao, K.-z.; Wang, L.-z. Morphology-dependent NiMoO4/carbon composites for high performance supercapacitors. *Inorg. Chem. Commun.* **2020**, *111*, 107631.
(10) Zhang, Y.; Yao, Q.-q.; Gao, H.-l.; Zhang, L.-s.; Wang, L.-z.; Zhang, A.-q.; Song, Y.-h.; Wang, L.-x. Synthesis and electrochemical performance of MnO2/BC composite as active materials for supercapacitors. *J. Anal. Appl. Pyrol.* **2015**, *111*, 233−237.
(11) Zhang, Y.; Gao, H.-l.; Jia, X.-d.; Wang, S.-w.; Yan, J.; Luo, H.-w.; Gao, K.-z.; Fang, H.; Zhang, A.-q.; Wang, L.-z. NiMoO4 nanorods supported on nickel foam for high-performance supercapacitor electrode materials. *J. Renew. Sustain. Energy* **2018**, *10*, 054101.
(12) Ghobashy, M. M.; Elkodous, M.; Shabaka, S. H.; Younis, S. A.; Alshangiti, D. M.; Madani, M.; Al-Gahtany, S. A.; Elkhatib, W. F.; Noreddin, A. M.; Nady, N.; El-Sayyad, G. S. An overview of methods for production and detection of silver nanoparticles, with emphasis on their fate and toxicological effects on human, soil, and aquatic environment. *Nanotechnol. Rev.* **2021**, *10*, 954−977.
(13) Zhang, Y.; Mei, H.-x.; Cao, Y.; Yan, X.-h.; Yan, J.; Gao, H.-l.; Luo, H.-w.; Wang, S.-w.; Jia, X.-d.; Kachalova, L.; Yang, J.; Xue, S.-c.; Zhou, C.-g.; Wang, L.-x.; Gui, Y.-h. Recent advances and challenges of electrode materials for flexible supercapacitors. *Coord. Chem. Rev.* **2021**, *438*, 213910. (a) Zhang, Y.; Xue, S.-c.; Yan, X.-h.; Gao, H.-l.; Jing, X.; Gao, K.-z.; Cao, Y.; Luo, H.-w.; Yan, J. Synthesis of CoAl-LDH@ Ni (OH) 2 high-performance supercapacitor electrode composites by hydrothermal-assisted electrodeposition. *Ionics* **2022**, *28*, 5211−5222.
(14) Florentin, Y.; Pearlmutter, D.; Givoni, B.; Gal, E. A life-cycle energy and carbon analysis of hemp-lime bio-composite building materials. *Energy and Buildings* **2017**, *156*, 293−305.
(15) Wernery, J.; Mancebo, F.; Malfait, W. J.; O'Connor, M.; Jelle, B. P. The economics of thermal superinsulation in buildings. *Energy Build.* **2021**, *253*, 111506.
(16) Yang, X.; Li, S.; Ye, D.; Kuang, J.; Guo, S.; Zou, Y.; Cai, X. Integrated Bifunctional Oxygen Electrodes for Flexible Zinc−Air Batteries: From Electrode Designing to Wearable Energy Storage. *Adv. Mater. Technol.* **2021**, *7*, 2100673.
(17) Ma, M.; Li, H.; Xiong, Y.; Dong, F. Rational design, synthesis, and application of silica/graphene-based nanocomposite: A review. *Mater. Des.* **2021**, *198*, 109367.
(18) Gu, W.; Sheng, J.; Huang, Q.; Wang, G.; Chen, J.; Ji, G. Environmentally friendly and multifunctional shaddock peel-based carbon aerogel for thermal-insulation and microwave absorption. *Nano-Micro Lett.* **2021**, *13*, 1−14. (a) Lee, J.-H.; Park, S. J. Recent advances in preparations and applications of carbon aerogels: A review. *Carbon* **2020**, *163*, 1−18.
(19) Ghobashy, M. M.; Elhady, M. A. Radiation crosslinked magnetized wax (PE/Fe3O4) nano composite for selective oil adsorption. *Compos. Commun.* **2017**, *3*, 18−22.
(20) Sharshir, A. I.; Fayek, S. A.; El-Gawad, A. F. A.; Farahat, M. A.; Ismail, M. I.; Ghobashy, M. M. Impact of γ-irradiation and SBR content in the compatibility of aminated (PVC/LLDPE)/ZnO for improving their AC conductivity and oil removal. *Sci. Rep.* **2022**, *12*, 19616.
(21) Ghobashy, M. M.; Khafaga, M. R. Chemical modification of nano polyacrylonitrile prepared by emulsion polymerization induced by gamma radiation and their use for removal of some metal ions. *J. Polym. Environ.* **2017**, *25*, 343−348.
(22) Ghobashy, M. M.; El-Damhougy, B. K.; El-Wahab, H. A.; Madani, M.; Amin, M. A.; Naser, A. E. M.; Abdelhai, F.; Nady, N.; Meganid, A. S.; Alkhursani, S. A.; Alshangiti, D. M. Controlling radiation degradation of a CMC solution to optimize the swelling of acrylic acid hydrogel as water and fertilizer carriers. *Polym. Adv. Technol.* **2021**, *32*, 514−524.
(23) Ghobashy, M. M.; Alshangiti, D. M.; Alkhursani, S. A.; Al-Gahtany, S. A.; Shokr, F. S.; Madani, M. Improvement of in vitro dissolution of the poor water-soluble amlodipine drug by solid dispersion with irradiated polyvinylpyrrolidone. *ACS Omega* **2020**, *5*, 21476−21487.
(24) Ghobashy, M. M.; El-Sattar, N. E. A. A. Radiation synthesis of rapidly self-healing hydrogel derived from poly (acrylic acid) with good mechanical strength. *Macromol. Chem. Phys.* **2020**, *221*, 2000218.
(25) Ghobashy, M. M.; Younis, S. A.; Elhady, M. A.; Serp, P. Radiation induced in-situ cationic polymerization of polystyrene organogel for selective absorption of cholorophenols from petro-chemical wastewater. *J. Environ. Manag.* **2018**, *210*, 307−315.
(26) Younis, S. A.; Ghobashy, M. M.; Samy, M. Development of aminated poly (glycidyl methacrylate) nanosorbent by green gamma radiation for phenol and malathion contaminated wastewater treatment. *J. Environ. Chem. Eng.* **2017**, *5*, 2325−2336.
(27) Othman, A. M.; Ghobashy, M. M.; Abd El-Sattar, N. E. A. Radiation synthesis of porous calcium silicate aerogel derived from polyacrylamide hydrogel as thermal insulator. *J. Sol-Gel Sci. Technol.* **2021**, *98*, 593−604.
(28) Ghobashy, M. M.; Abd El-Wahab, H.; Ismail, M. A.; Naser, A. M.; Abdelhai, F.; El-Damhougy, B. K.; Nady, N.; Meganid, A. S.; Alkhursani, S. A. Characterization of Starch-based three components of gamma-ray cross-linked hydrogels to be used as a soil conditioner. *Mater. Sci. Eng., B* **2020**, *260*, 114645.
(29) Ghobashy, M. M.; El-Damhougy, B. K.; Nady, N.; El-Wahab, H. A.; Naser, A. M.; Abdelhai, F. Radiation crosslinking of modifying super absorbent (polyacrylamide/gelatin) hydrogel as fertilizers carrier and soil conditioner. *J. Polym. Environ.* **2018**, *26*, 3981−3994.
(30) Gan, G.; Li, X.; Fan, S.; Wang, L.; Qin, M.; Yin, Z.; Chen, G. Carbon Aerogels for Environmental Clean-Up. *Eur. J. Inorg. Chem.* **2019**, *2019*, 3126−3141.
(31) Yamamoto, T.; Nishimura, T.; Suzuki, T.; Tamon, H. Control of mesoporosity of carbon gels prepared by sol−gel polycondensation and freeze drying. *J. Non-Cryst. Solids* **2001**, *288*, 46−55.
(32) Wang, H.-L.; Cui, J.-Y.; Jiang, W.-F. Synthesis, characterization and flocculation activity of novel Fe (OH) 3−polyacrylamide hybrid polymer. *Mater. Chem. Phys.* **2011**, *130*, 993−999.
(33) Amonkosolpan, J.; Wolverson, D.; Goller, B.; Polisski, S.; Kovalev, D.; Rollings, M.; Grogan, M. D. W.; Birks, T. A. Porous silicon nanocrystals in a silica aerogel matrix. *Nanoscale Res. Lett.* **2012**, *7*, 397.
(34) Yan, B.; Liu, S.; Chastain, M. L.; Yang, S.; Chen, J. A new FTIR method for estimating the firing temperature of ceramic bronze-casting moulds from early China. *Sci. Rep.* **2021**, *11*, 1−10.
(35) Yang, G.; Jiang, Y.; Feng, J.; Zhang, S.; Feng, J. Synthesis of fibre reinforced Al2O3− SiO2 aerogel composite with high density uniformity via a facile high-pressure impregnation approach. *Process. Appl. Ceram.* **2017**, *11*, 185−190. (a) Cai, H.; Jiang, Y.; Feng, J.; Zhang, S.; Peng, F.; Xiao, Y.; Li, L.; Feng, J. Preparation of silica aerogels with high temperature resistance and low thermal conductivity by monodispersed silica sol. *Mater. Des.* **2020**, *191*, 108640. (b) He, J.; Li, X.; Su, D.; Ji, H.; Qiao, Y. High-strength mullite fibers reinforced ZrO 2−SiO 2 aerogels fabricated by rapid gel method. *J. Mater. Sci.* **2015**, *50*, 7488−7494.
(36) Guo, D.; Shibuya, R.; Akiba, C.; Saji, S.; Kondo, T.; Nakamura, J. Active sites of nitrogen-doped carbon materials for oxygen reduction reaction clarified using model catalysts. *Science* **2016**, *351*, 361−365.
(37) Shan, H.; Li, X.; Cui, Y.; Xiong, D.; Yan, B.; Li, D.; Lushington, A.; Sun, X. Sulfur/nitrogen dual-doped porous graphene aerogels enhancing anode performance of lithium ion batteries. *Electrochim. Acta* **2016**, *205*, 188−197.
(38) Kang, E. S.; Kim, Y.-W.; Nam, W. H. Multiple thermal resistance induced extremely low thermal conductivity in porous SiC-SiO2 ceramics with hierarchical porosity. *J. Eur. Ceram. Soc.* **2021**, *41*, 1171−1180.

https://doi.org/10.1021/acsomega.2c07335
ACS Omega 2023, 8, 20283−20292